Journal of Physics: Conference Series **614** (2015) 012009 doi:10.1088/1742-6596/614/1/012009

Detailed Study of Structural and Ferroelectric Properties in $BaTiO_3/La_{2/3}Ca_{1/3}MnO_3$ Bilayers Deposited by Pulsed Laser Deposition

JE Ordoñez[1], ME Gomez[1], W Lopera[1], and P Prieto[1,2]
[1] Department of Physics, Universidad del Valle, A. A. 25360 Cali, Colombia
[2] Center of Excellence for Novel Materials - CENM, Universidad del Valle, A. A. 25360 Cali, Colombia
E-mail: john.ordonez@correounivalle.edu.co

Abstract. We have deposited ferroelectric $BaTiO_3$ (BTO), and ferromagnetic $La_{2/3}Ca_{1/3}MnO_3$ bilayers on $SrTiO_3$ substrates by pulsed laser deposition at pure oxygen atmosphere and substrate temperature of 820 °C, keeping fixed the magnetic layer thickness (t_{LCMO}) at 50 nm and varying the thickness of the ferroelectric layer (t_{BTO}) from 20 to 100 nm. X-ray diffraction analysis indicates a textured growth of both layers. The lattice parameter of the $La_{2/3}Ca_{1/3}MnO_3$ layer is slightly modified by the presence of the $BaTiO_3$ layer. Resistivity versus temperature Arrhenius plots show a small polaron thermally activated conductivity in bilayers with activation energies from 120 to 135 meV. Polarization loops at the $BaTiO_3$ measured at room temperature, using the $La_{2/3}Ca_{1/3}MnO_3$ layer as bottom electrode, show a maximum remnant polarization of 20 $\mu C/cm^2$ and minimal coercive field of 70 kV/cm. Thus, the bilayers maintain marked ferroelectric and ferromagnetic properties on individual layers.

Key words: Ferroelectric films, magnetic multilayers, magnetic properties.

1. Introduction

Multiferroic materials exhibit, simultaneously, two or more "ferroic" properties, *i.e.*, ferroelectricity (FE), ferromagnetism (FM), ferroelasticity, or ferrotoroidicity [1]. Thus, these compounds are potentially interesting for technological applications and for the study of magnetoelectric interactions. Moreover, the multiferroic property in most of the compounds exists below room temperature, limiting the practical applications. Given that both saturation magnetization and polarization are comparatively small in most intrinsic multiferroics [2,3], considerable research activity has focused on extrinsic or hybrid multiferroics based on manganites and ferroic oxides showing interesting results [4-6]. For instance, we studied the electrical and magnetic properties of ferromagnetic $La_{2/3}Ca_{1/3}MnO_3$ (LCMO) and ferroelectric $BaTiO_3$ (BTO) bilayers and their dependence on BTO thickness, maintaining constant LCMO thickness at 50 nm [7]. We observed a variation of ferromagnetic parameters like saturation magnetization and coercive field, which has been attributed to spin canting and phase separation at the BTO/LCMO interface and strain-induced magnetic disorder in the film. For a 20-nm BTO thickness, all these effects were stronger; as BTO thickness increases, the stresses at both BTO and LCMO layers is relaxed and magnetization is closer to that for an LCMO film [7]. Additionally, LCMO/BTO bilayers deposited onto $Nb:SrTiO_3$ show that the presence of a BTO film on the bilayer enhances the metal-insulator transition, T_{M-I}, probably because the strains in the LCMO


Content from this work may be used under the terms of the Creative Commons Attribution 3.0 licence. Any further distribution of this work must maintain attribution to the author(s) and the title of the work, journal citation and DOI.
Published under licence by IOP Publishing Ltd

layer in the bilayer are lower than those induced when the LCMO film grows directly on the substrate. When t_{BTO} increases the strains in the structure relax, allowing release of tension in the magnetic LCMO layer and improving conduction properties [8]. In this paper we report structural and ferroelectric properties of $BaTiO_3$ (t_{BTO})/$La_{2/3}Ca_{1/3}MnO_3$ (t_{LCMO})/$SrTiO_3$-substrate, when LCMO thickness is fixed (at 50 nm) and BTO thickness varies by 20, 50, and 100 nm. Transport properties were analyzed by using a small polaron model, from where activation energies were calculated. Ferroelectric properties were studied in an Au/BTO/LCMO structure at room temperature. The $BaTiO_3$ (t_{BTO})/$La_{2/3}Ca_{1/3}MnO_3$ (t_{LCMO})/$SrTiO_3$ bilayer exhibits both: ferroelectric and ferromagnetic behavior.

2. Experimental

$BaTiO_3$ (t_{BTO})/$La_{2/3}Ca_{1/3}MnO_3$ (t_{LCMO}) bilayers were deposited onto (001) single-crystal $SrTiO_3$ substrates via pulsed laser deposition (PLD) at pure O_2 atmosphere at a pressure around 10^{-3} Torr and substrate temperature of 820 °C. An excimer laser (KrF) operating at 248 nm, 10 Hz and 20-50 mJ was used. We chose three different values for the BTO thickness: 20, 50, and 100 nm, that is, t_{BTO}/t_{LCMO} is around ½, 1/1 and 2/1, respectively. The crystal structure was studied by X-ray diffraction (XRD) using a BRUKER diffractometer with Cu K_α wavelength at θ-2θ scans and rocking curves. Magnetotransport measurements were carried out in a Physical Property Measurement System (Quantum Design - PPMS–6600) in the range of 10 to 300 K. Resistance, as a function of temperature, was measured by the standard four-probe technique with current-in-plane (CIP) geometry. Magnetoresistance (MR) was examined with an applied magnetic field (H) of up to 20 kOe, perpendicular to the current direction and perpendicular to the plane. In order to compare the temperature dependence of the resistance curves, we normalized the resistance (for H = 0) at the transition temperature. For MR, we used the expression MR = R(H)/R(H=0), where R(H=0) is the resistance value at H=0 at the transition temperature. Ferroelectric hysteresis loops were carried out with an RT66B test system (Radiant Technologies) using a micromanipulator to contact the samples. Measurements were normalized with ferroelectric BTO thickness, and fatigue test show polarization cycling dependence.

3. Results

3.1. Structural and morphological properties

Figure 1 shows the out-of-plane XRD θ-2θ scans for BTO (t_{BTO})/LCMO (50 nm) bilayers grown on STO substrates, with t_{BTO} = 20, 50, and 100 nm nominal thickness. We observed the LCMO- and BTO-(00l) diffraction peaks around the (001) and (002) substrate Bragg reflections, indicating a texture growth of both layers with the [00l] direction perpendicular to the substrate surface. Interestingly enough, the LCMO Bragg reflex in the bilayer coincides with that for the LCMO film (dotted line) grown on STO under identical parameters. Thus, there is no effect of the BTO layer on the position of the Bragg reflex for the LCMO layer. However, the width of the (00l) BTO peaks depends on its thickness being wider for the sample with t_{BTO} = 20 nm. This could indicate that for small BTO thicknesses, X-ray scans detect strains that will relax when the BTO thickness increases, and the peak is then less wide. The full width at half maximum (FWHM) of each layer in a bilayer were 0.028° and 0.09° for LCMO (50 nm) and BTO (50 nm), respectively (Fig. 1d, and 1e), which are good values for these kinds of samples and show the high quality of the bilayers obtained. The width of the rocking curve for the LCMO in a bilayer is greater than that for a 50-nm LCMO/STO film, probably because the LCMO in the bilayer is anchored at the bottom with the substrate and at the top with the BTO layer. Figure 1-f shows the BTO and LCMO lattice parameter dependence on BTO thickness. Dotted lines are plots for the *c* and *a* lattice parameters in bulk BTO; *c* substrate lattice parameter; the *c* lattice parameter in LCMO bulk and film. Plots indicate that the *c*-LCMO lattice parameter in the bilayer shifts slightly compared to that for a 50-nm LCMO/STO film, and it is independent from the thickness of the BTO layer. The *c*-BTO lattice parameter is above the BTO bulk, as expected for this thin-film material. It shows a non-monotonic decrease with increased BTO thickness, probably due to strain relaxation.

3.2. Transport properties

Figure 2a shows the dependence of ln(*R*/*T*) on 1/*T* (Arrhenius plot) for BTO(t_{BTO})/LCMO(50 nm) bilayers grown on STO substrate, with BTO thickness of t_{BTO} = 20 nm (open square symbol), 50 nm (open circle symbol), 100 nm (open pentagon symbol). Temperature dependence plots are the typical for the LCMO films. In the high temperature range, the curves can be described on the basis of small polaron thermally activated conductivity (SPTAC), which predicts an expression $R(T)=R_0 T\exp(E_a/k_B T)$, where E_a is the activation energy in electron volts, and k_B is the Boltzmann constant [9-11]. From the fitting of the experimental data to this expression, we calculated the activation energy. E_a decreases with increased BTO thickness (Fig. 2b). The activation energy in these bilayers is smaller than that for a 50-nm LCMO/STO film (144 meV, dotted line in plot). Changes in the activation energy, E_a, can be explained by the significant difference in the Mn–O–Mn angle in LCMO octahedra, which plays a key role for the transport mechanism in manganites [12]. We have obtained values for E_a in the range between 120 and 135 meV. It indicates that the presence of a BTO layer modifies the activation energy of the hopping conduction in the LCMO layer and may be changing the Mn-O-Mn angles in the octahedra.

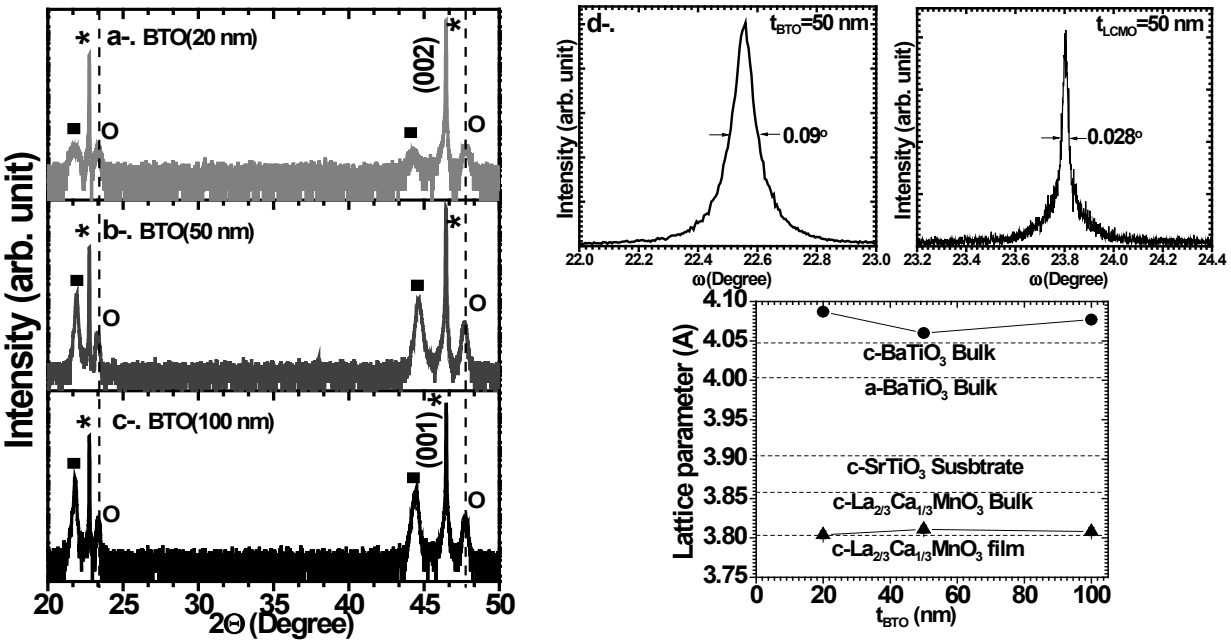

Figure 1. X-ray diffraction patterns for BTO/LCMO bilayers grown on (001) $SrTiO_3$ for a-. BTO (20 nm)/LCMO (50 nm), b-. BTO (50 nm)/LCMO (50 nm), and c-. BTO (100 nm)/LCMO (50 nm). Peaks are marked with open circles for LCMO, full squares for BTO, and asterisks for the STO substrate. d-. Rocking curve around BTO (002) peak for t_{BTO} = 50 nm with a FWHM = 0.09°, e-. Rocking curve around LCMO (002) peak for t_{LCMO} = 50 nm with a FWHM = 0.028°, f-. BTO (closed circles) and LCMO (closed triangles) lattice parameter dependence on BTO thickness. Lines are guides to the eye.

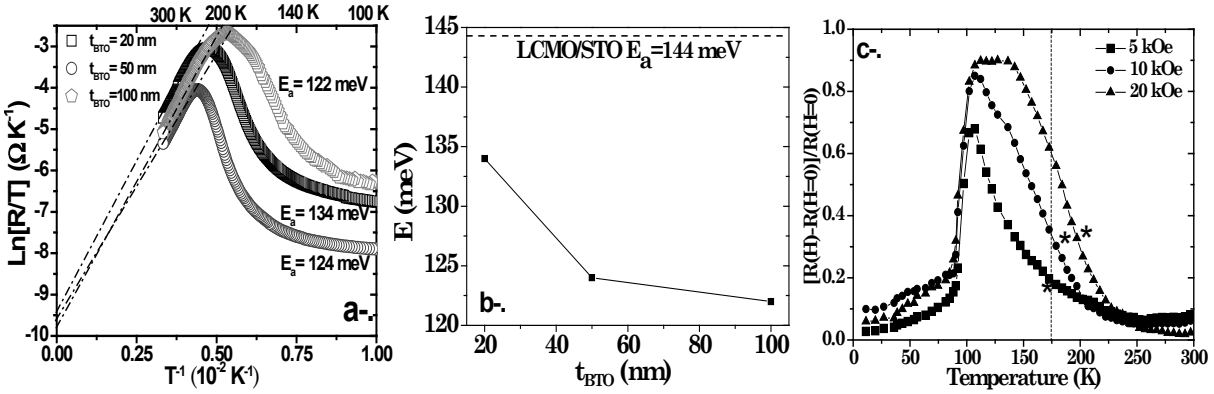

Figure 2. a-. Arrhenius plots for the BTO (t_{BTO})/LCMO (50 nm) bilayers, t_{BTO}=20 nm (open squares), t_{BTO} = 50 nm (open circles), and t_{BTO} = 100 nm (open pentagon); the dotted lines are fitting curves based on the SPTAC model. b-. Activation energy as function of BTO layer thickness (lines are guides for the eye). c-. Magnetoresistance dependence on temperature for the BTO (100 nm)/LCMO (50 nm) bilayer at applied magnetic field of 5 kOe (squares), 10 kOe (circles), and 20 kOe (triangles). Temperature for the metal insulator transition is marked with asterisks. Dotted line indicates the temperature for the metal-insulator transition (MIT) for a 50-nm LCMO film grown on (001) STO.

Figure 2c displays the temperature dependence of magnetoresistance for BTO (100 nm)/LCMO (50nm) bilayer at applied magnetic fields of 5kOe (circles), 10 kOe (squares), 20 kOe (pentagons). We have defined magnetoresistance as MR = [R(0) − R(H)]/R(0). Resistance has been measured in CIP geometry; R (H=0) and R(H) are the resistances with and without a magnetic field. In the Plots we mark with asterisks the temperature at which the MIT takes place. In all bilayers, the temperature for the MIT increases with increased applied magnetic field. This behavior is usual in optimal doped manganite [13, 14]. The temperature for the MIT is smaller than that for H=0 and that for a 50-nm LCMO film, indicating that the presence of the BTO layer affects conduction in the LCMO layer because of local structural changes at the interfaces causing competition between phases increasing the MI-width of the transition. We measured resistance in the in-plane geometry, thus, we have contributed to resistance from the BTO layer and the LCMO-BTO interface that we cannot elucidate in this kind of measurement. Magnetotransport properties are extremely sensitive to changes in double-exchange interactions, which are, in turn, strongly affected by the variations in the angles between MnO_6 octahedra induced by strain [13] at BTO/LCMO and LCMO/STO interfaces or by changes in TiO_6 octahedra crystal field.

We performed ferroelectric measurements on the Au/BTO (20-100 nm)/LCMO (50 nm) structures, using the LCMO layer as bottom electrode and Au as top electrode. Hysteresis loops were measured at room temperature, at 1-kHz frequency. Measurements were carried out under 350 kV/cm applied electric field. Figures 3a and 3b show the room-temperature ferroelectric hysteresis loops P–E for Au/BTO/LCMO structures. Both remnant polarization and coercive electric field depend on the BTO thickness. Remnant polarizations were 13, 20, and 18 μC/cm^2 and the coercive fields were 180, 103, and 70 kV/cm for t_{BTO} = 20, 50, and 100 nm, respectively, after one cycle. For the thinnest BTO layer, the remnant polarization is the smallest and coercive field is the biggest. It could indicate that, for the thin BTO layer, the electrical dipolar moment is probably diminished at the interfaces and its contribution to polarization density is smaller; whereas, the field necessary for polarization reversal increases with decreased thickness because of the strained layer that increases the pinning energy. The LCMO layer shows good performance as bottom electrode for ferroelectric measurements.

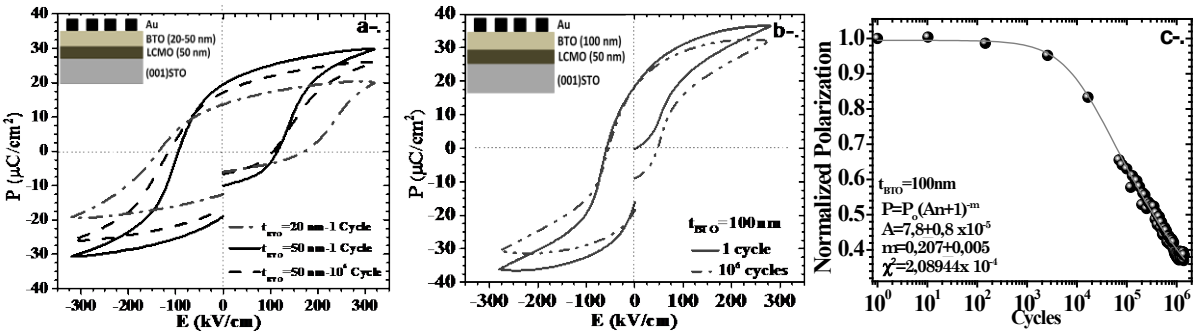

Figure 3 a-. P–E hysteresis loops at room temperature for Au/BTO(20-50 nm)/LCMO/STO. t_{BTO} = 20 nm after one cycle (dash dot), t_{BTO} = 50 nm after one cycle (solid), and t_{BTO} = 50 nm after 10^6 cycles (dash). b-. P–E hysteresis loops at room temperature for Au/BTO(100 nm)/LCMO/STO. t_{BTO} = 100 nm after one cycle (solid) and 10^6 cycles (dash dot dot). Upper inset shows the system configuration. c-. Fatigue test: normalized polarization vs. number of cycles. Solid line is the fitted curve to a $P=P_o(A_n+1)^{-m}$ theoretical model.

We performed fatigue measurements after 10^6 cycles. Figure 3c shows fatigue measurements for an Au/BTO (100 nm)/LCMO (50 nm) structure at room temperature. Normalized polarization decreases slightly with the number of cycles, but after a certain value of cycles it decreases dramatically. The behavior fit with the Yoo and Desu model [15], according to the expression $P = P_o(A_n+1)^{-m}$, for this case pilling constant $A = 7.8 \pm 0.8 \times 10^{-5}$ and decay exponent $m = 0.207 \pm 0.005$ with $\chi^2 = 2,09 \times 10^{-4}$. The effect basically consists in that for low frequencies, the oxygen vacancies will start to migrate and the trapped charges will gradually respond to the applied voltage. The rearrangement of the oxygen vacancies will affect the ferroelectric domains, impeding their switching and leading to a considerable decrease in the polarization value. The rearrangement will end after a certain number of cycles and then a recovery process might start. Recovery can occur if the amount of the charged defects acting as pinning centers for the ferroelectric domains is reduced [16,17].

4. Conclusions

We successfully produced a multiferroic hybrid system based on ferroelectric/ferromagnetic bilayers of oxide materials by using BTO as ferroelectric, and LCMO as ferromagnetic layer. The position of the Bragg reflections for LCMO films in bilayers are not modified for the presence of BTO, but the width of the (00l) BTO peaks depends on their thickness, being wider for small thicknesses, which could be related to the presence of strains that relax when BTO thickness increases. The presence of BTO layers modifies the activation energy of the hopping conduction in the LCMO layers. This can be carried out by changing the Mn-O-Mn angles in the octahedra. The metal insulator transition in LCMO layer is affected by the BTO layer because local structural changes at the interfaces can produce competition among phases, increasing the MI-width of the transition. Ferroelectric properties of bilayers show a dependence with BTO layer thickness, where for the thinnest BTO layer the remnant polarization is the smallest and coercive field is the biggest, which could indicate that for thin BTO layers, the electrical dipolar moment is probably diminished at the interfaces and its contribution to polarization density is smaller, whereas the field necessary for the polarization reversal increases with decreased thickness because of the strained layer that increases the pinning energy.

5. Acknowledgments

This work was financially supported by *"Instituto de Nanociencia de Aragón"*, Zaragoza, Spain, where the films were grown and partially characterized; the Center of Excellence for Novel Materials (CENM), COLCIENCIAS research projects: "Study of structural and physical properties in oxide materials and interfaces as potential sensor and control systems"; No 110656933104 contract No.2013-0002 CI 7917-CC 10510 COLCIENCIAS-UNIVALLE and "Study of interface phenomena in heterostructures based on complex oxides" CI 7978 UNIVALLE.

6. References

[1] Martin L, Chu Y-H, and Ramesh R 2010 *Mat. Sci. Eng R*, **68**, 89.
[2] Chu Y-H, Martin L, Holcomb M., Gajek M, Han S-J, He Q, Balke N, Yang C-H, Lee D, Hu W, Zhan Q, Yang P, Fraile-Rodríguez A, Scholl A, Wang S and Ramesh R (2008), Nat. Mater. vol 7, pp 478 – 482.
[3] Ramesh R and Spaldin N A (2007), "Multiferroics: progress and prospects in thin films", Nat. Mater. Vol. 6, pp. 21-29.
[4] Li T, Zhang F, Fang H, Li K, Yu F (2013), Journal of Alloys and Compounds 560, pp. 167–170.
[5] Burton J D, Tsymbal E Y (2009), Phys. Rev. B 80, 174406.
[6] Ziese M (2008), J. Appl. Phys. Vol. 104, 063908/1-9.
[7] Ordoñez J E, Gómez M E, Lopera W, Prieto P (2013), IEEE Transactions on Magnetics, VOL. 49, NO. 8, pp. 4586-4589.
[8] Ordoñez J E, Gómez M E, Lopera W, Prieto P (2014), Journal of Physics: Conference Series, Volume 480, Issue 1, pp. 1-4.
[9] Navasery M, Halim S A, Dehzangi A, Soltani N, Bahmanrokh G, Erfani M, Kamalianfar A, Pan K Y, Chang S C, Chen S K, Lim K P, Awang Kechik M M, Applied Physics A, Online First, doi: 10.1007/s00339-014-8295-5.
[10] El Helali S, Daoudi K, Fouzri A, Oumezzine M, OueslatiM and Tsuchiya T (2012), Appl Phys A, vol. 108, pp. 379–384.
[11] Prokhorov V G, Komashko V A, Kaminsky G G, Svetchnikov V L, Zandbergen H W, Lee Y P, Park J S and Kim K W (2003), Low Temp. Phys. Vol. 29, pp. 117-122.
[12] Amaral V S, Lourenço A A C S, Araújo J P, Pereira A M, Sousa J B (2000), J. Appl. Phys., Vol. 87, No. 9, 1.
[13] Dagotto E, Hott T and Moreo A 2001 *Phys. Rep.*, **344**, 1.
[14] Li X, Li K, Du J, Xu X, Fang J, Wang Z, Cao X, Zhu J, Zhang Y (1998), Science in China Series A: Mathematics, Vol. 41, Issue 3 , pp 308-312.
[15]Yoo I K and Desu S B (1992), phys. Stat. sol. (a), Vol. 133, Issue 2, pp. 565-573.
[16] Scott J F and Dawber M (2000), Appl. Phys. Lett. 76, 3801-3803.
[17] Pintilie L, Vrejoiu I, Hesse D, and Alexe M (2006), Appl. Phys. Lett. 88.